Geochemistry of pyrite from diamictites of the Boolgeeda Iron Formation, Western Australia with implications for the GOE and Paleoproterozoic ice ages ☆

Elizabeth D. Swanner [a,1], Andrey Bekker [b], Ernesto Pecoits [c], Kurt O. Konhauser [c], Nicole L. Cates [a], Stephen J. Mojzsis [a,d,e,*]

[a] Department of Geological Sciences, University of Colorado, UCB 399, 2200 Colorado Avenue, Boulder, CO 80309-0399, USA
[b] Department of Geological Sciences, University of Manitoba, Winnipeg, Manitoba R3T 2N2, Canada
[c] Department of Earth and Atmospheric Sciences, University of Alberta, Edmonton, Alberta T6G 2E3, Canada
[d] Institute for Geological and Geochemical Research, Research Centre for Astronomy and Earth Sciences, Hungarian Academy of Sciences, Budapest, Budaorsi ut 45, H-1112, Hungary
[e] Laboratoire de Géologie de Lyon, Ecole Normale Supérieure de Lyon and Université Claude Bernard Lyon 1, CNRS UMR 5276, 46 Allée d'Italie, 69007 Lyon, France

ARTICLE INFO

ABSTRACT

Sediments of the ca. 2400 Ma Turee Creek Group of Western Australia are coincident with the oxygenation of Earth's surface associated with the 'Great Oxidation Event' (GOE). Diamictite within the Boolgeeda Iron Formation from the Boundary Ridge section at the Duck Creek Syncline was previously correlated to the glaciogenic sediments of the Meteorite Bore Member of the Turee Creek Group at the Hardey Syncline (Martin, 1999). The Meteorite Bore Member is considered correlative and time-equivalent with the Paleoproterozoic glacial diamictites of the 2.45–2.22 Ga Huronian Supergroup in North America. If the diamictite units at Boundary Ridge correspond to worldwide Paleoproterozoic glaciations, they should also record the disappearance of mass independently fractionated (MIF) sulfur. Triple S-isotope compositions for pyrites from the Boundary Ridge sections were measured in situ by a multi-collector ion microprobe and yielded both mass dependently fractionated (MDF) and MIF sulfur isotope values ($\Delta^{33}S$ values from -0.44 to $+6.27‰$). Trace element heterogeneities are indicated by measurements at multiple spatial scales within rounded pyrites in the Boundary Ridge section, consistent with multiple generations of pyrite that incorporated sulfur processed in an anoxic atmosphere. A compilation of S-isotope data from pyrite in the Boundary Ridge diamictites analyzed in this study and previous work (Williford et al., 2011) defines multiple $\delta^{34}S$ vs. $\delta^{33}S$ arrays, consistent with an origin of detrital pyrite from the underlying Hamersley and Fortescue groups. Sulfides in a shale unit from the Boundary Ridge section plot along the terrestrial fractionation line but still retain positive MIF-S. This and detrital pyrite suggest low atmospheric oxygen immediately before the initiation of Paleoproterozoic Ice Ages. This data is inconsistent with a correlation to glacially-influenced successions within the North American Huronian Supergroup, in which the MIF-S signal permanently disappears. The diamictites at the Duck Creek Syncline are older than the Meteorite Bore Member because their stratigraphic position is within the Boolgeeda Iron Formation that underlies the Turee Creek Group, which is separated from the Meteorite Bore Member by nearly 1000 m of the Kungarra shale at the Hardey Syncline.

1. Introduction and geological setting

The principal geochemical indicators used to probe conditions for marine pyrite (FeS_2) formation in the Archean and Paleoproterozoic are multiple sulfur isotopes (^{32}S, ^{33}S, ^{34}S and ^{36}S), iron isotopes (typically ^{54}Fe and ^{56}Fe; although ^{57}Fe and ^{58}Fe have been also used), and variable trace metal concentrations (Ni, Co, and other transition metals). The Archean Eon (ca. 3850 to 2500 Ma) affords special opportunities to identify various sulfur sources to sedimentary pyrite because before about 2400 Ma the sulfur isotopic compositions of marine (and presumably lacustrine) sedimentary sulfide and sulfate minerals record mass-independent fractionation with the relationship $\delta^{33}S \neq 0.515 \cdot \delta^{34}S$

that is imparted by deep-UV photolysis of SO–SO$_2$ from volcanic gases processed in an anoxic atmosphere (Farquhar et al., 2000; Pavlov and Kasting, 2002; Bekker et al., 2004). Sulfate aerosols and SO$_2$ ($+\Delta^{33}$S), and S$_8$ aerosols, H$_2$S and HS ($-\Delta^{33}$S), were an important source of MIF-S to the ocean, and accounted for 1–2% of the sedimentary sulfur budget (Farquhar and Wing, 2003). This MIF-S is widely preserved in authigenic Archean marine pyrite, and can be used to differentiate microbial and abiotic pathways of sulfur cycling and to identify the sulfur source at time of deposition (Mojzsis, 2007; Philippot et al., 2007, 2012; Ueno et al., 2008). Moreover, patterns in δ^{34}S, δ^{33}S and Δ^{33}S values of detrital pyrite in Archean siliciclastic sediments reflect composition of the source (Hofmann et al., 2009). Multiple sulfur isotope data in ancient sulfides substantially augments the information provided by pyrite textures, morphologies and elemental composition in determining the source of sulfur in pyrite and the environmental processes by which it formed, and is now routinely employed in analysis of ancient sediments.

The disappearance of MIF-S from the pyrite record before about 2300 Ma occurred in the context of what is regarded as an epoch of Paleoproterozoic "Snowball Earth" events, a name coined for worldwide ice ages that extended to low latitudes (Kirschvink, 1992). It has been suggested that the Paleoproterozoic ice ages were accompanied by fluctuations in the atmospheric oxygen level; the rise of atmospheric oxygen led to decrease in atmospheric methane, a strong greenhouse gas in the Archean, and thence to global glaciation (Kirschvink et al., 2000). Atmospheric oxygen levels fell during these glaciations, which resulted in higher CO$_2$ and methane levels, greenhouse feedback and subsequent deglaciation (Bekker and Kaufman, 2007). The Espanola Formation of the 2.45–2.22 Ga Huronian Supergroup records a large range in δ^{34}S values of MDF sulfur that was interpreted to reflect the onset of atmospheric oxidation in the Paleoproterozoic (Papineau et al., 2007). In addition, the underlying McKim and Pecors formations also show attenuated range of MIF in sulfur isotopes of sedimentary sulfides (Wing et al., 2002, 2004; Papineau et al., 2007). Glacial diamictite-bearing sediments of the South African Duitschland Formation, which also record the disappearance of MIF sulfur (Bekker et al., 2004; Guo et al., 2009), seem to correlate to the Espanola Formation of the Huronian successions (Bekker et al., 2001). The widespread presence of glacial diamictites of broadly similar age has been used to support the contention that worldwide Paleoproterozoic "Snowball Earth" glaciations occurred at that time. Despite the apparent correlations between Paleoproterozoic glacially-influenced sedimentary successions across two continents, it remains a subject of debate whether or not these glacial diamictites correspond to the same global environmental event (Kopp et al., 2005).

The ca. 2420 Ma Turee Creek Group in Western Australia (Fig. 1) encompasses sediments deposited during the GOE. The Turee Creek Group conformably overlies the Boolgeeda Iron Formation, is underlain by the 2449 ± 3 Ma Wongarra rhyolite (Barley et al., 1997) and is intruded by 2208 ± 10 Ma mafic sills (Müller et al., 2005). A maximum depositional age of ca. 2420 Ma was recently established from age data derived from detrital zircons within the Meteorite Bore Member of the Turee Creek Group (Takehara et al., 2010). Diamictites from the Meteorite Bore Member at the Hardey Syncline host striated clasts of probable glacial origin, and have been broadly correlated to the Paleoproterozoic glacial deposits from the Huronian Supergroup in North America and Transvaal Supergroup in South Africa (Trendall, 1981). However, the Meteorite Bore Member at the Hardey Syncline is truncated by an unconformity and has a strong penetrative cleavage (Trendall, 1981; Krapez, 1996; Krapež et al., 2003), necessitating interrogation of samples from other potentially correlative, but less deformed areas.

Diamictite horizons at the Duck Creek Syncline and at Yeera Bluff occur within the Boolgeeda Iron Formation, and were previously correlated with the glaciogenic diamictite of the Meteorite Bore Member (Martin, 1999). If the Meteorite Bore Member correlates to diamictites in the Boolgeeda Iron Formation, and if the Meteorite Bore Member

represents the Australian record of these purported global glaciations, then the sedimentary pyrites from the Boolgeeda Iron Formation should show a similar pattern of multiple sulfur isotope variations with a general progression from large to attenuated range of MIF culminating in the irreversible transition to MDF-S as documented in glacial successions within the North American Huronian Supergroup and the South African Transvaal Supergroup cited above. Previous analyses reported for authigenic and detrital pyrites within diamictite horizons of the Boolgeeda Iron Formation from the Duck Creek Syncline at Boundary Ridge and at the Deepdale locality near Yeera Bluff apparently did not show such a trend (Williford et al., 2011). Here, we re-examine the argument that the Meteorite Bore Member glacial diamictite is recorded in the Boundary Ridge and the Deepdale locations by significantly expanding the database of trace element compositions and multiple sulfur isotope measurements of pyrite within these samples. The syngenicity and also synchronicity of the diamictites from the Boolgeeda Iron Formation with Paleoproterozoic glacial sediments elsewhere that span the GOE can therefore be tested by comparison of the multiple sulfur isotope composition of authigenic pyrites to existing records from the Huronian Supergroup in North America and the Transvaal Supergroup in South Africa.

The GOE might have been preceded by a geologically protracted time interval of progressive surface oxygenation marked by transient oxygenation events, the so-called 'whiffs' (e.g., Anbar et al., 2007; Papineau et al., 2007; Kaufman et al., 2007). It is plausible that oxidative continental weathering emerged before the disappearance of MIF-S from the rock record (Konhauser et al., 2011), since sulfate delivered to the ocean from the continents when sulfides were oxidized for the first time is expected to carry MIF (Farquhar and Wing, 2003). The average Δ^{33}S value of the Archean continental crust is poorly known, but available data for Archean sedimentary sulfides and sulfates show a clear bias towards positive values (Mojzsis et al., 2003; Farquhar and Wing, 2003; Mojzsis, 2007; Halevy et al., 2010; Johnston, 2011). If this was the case, the S isotope signature of this transition time interval ought to be manifested in a larger range of δ^{34}S values reflecting an increase in seawater sulfate reservoir, and a limited range of positive Δ^{33}S values corresponding with the average value of the Archean continental crust. A large range of δ^{34}S values and a stratigraphically-persistent, narrow range of small to moderately positive Δ^{33}S values are expected once oxidative weathering of continental crust took over leading to or during the early stage of the GOE (Reinhard et al., 2013). The Turee Creek Group sediments as well as other sedimentary successions straddling the GOE could provide a test for this prediction.

2. Samples and methods

2.1. Samples associated with diamictites in the Hamersley Province

Samples with observable pyrite earmarked for multiple sulfur isotope analysis and trace element studies were collected from two diamictite localities within the Boolgeeda Iron Formation in the westernmost part of the Hamersley Province (Fig. 1a) in April 2008 by M. Van Kranendonk and S.J. Mojzsis. Most samples came from the diamictite-bearing sequence in the Duck Creek Syncline at a locality known as Boundary Ridge (S-22°30′53.28″, W-116°31′12.37″). Samples analyzed from the Boundary Ridge location include a sandstone bed (190569 and 190583; Fig. 1b), a sandstone bed with scattered clasts, occasional outsized clasts (lonestones; 190578) and an overlying fissile shale (190575) with pebble to boulder-sized clasts (Williford et al., 2011; Hickman and Van Kranendonk, 2012). One additional sample is from the diamictite-bearing Deepdale section from a similar stratigraphic position (S-21°42′26.55″, W-116°08′23.66″), which corresponds to the "Yeera Bluff" location as described in Martin (1999). The Deepdale section is an outcrop of the Boolgeeda Iron Formation west of the Deepdale homestead, and the upper part of the formation is
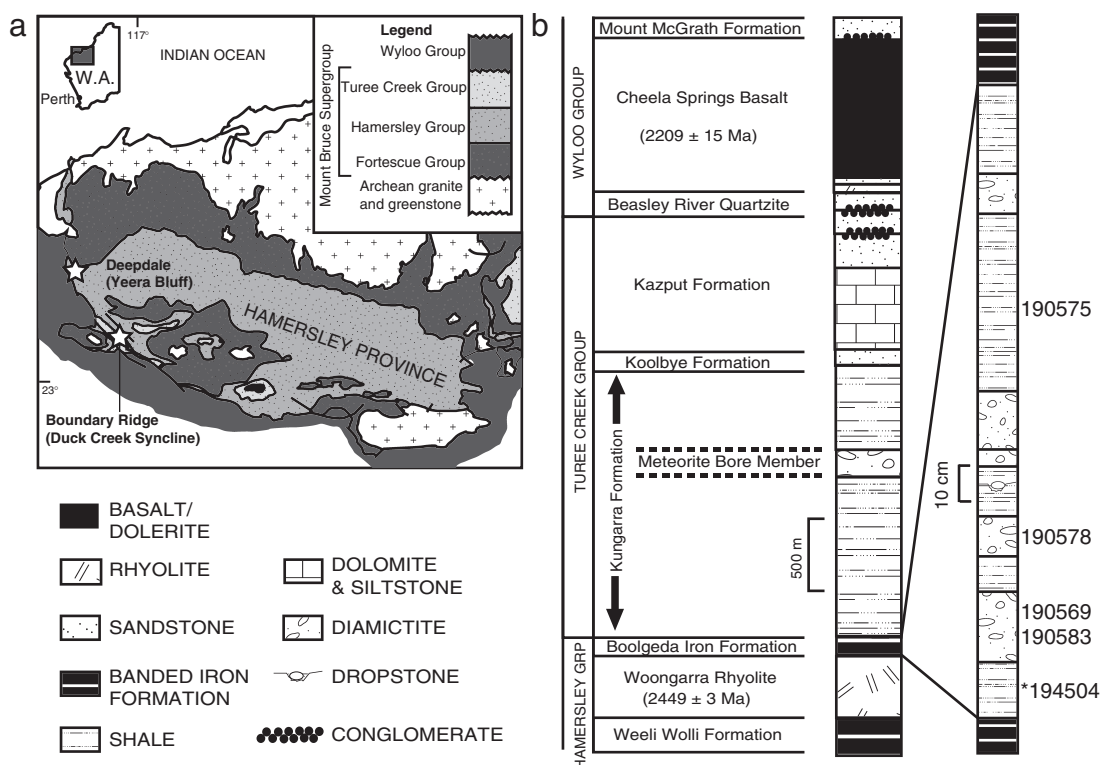
Fig. 1. a. Geologic map of Western Australia, showing the southwestern Hamersley Province and sampled locations (✩). b. Lithostratigraphy of the Meteorite Bore Member at the Hardey Syncline (left column) and the Boundary Ridge sampling location at the Duck Creek Syncline (right column). The samples are from sandstone and shale/mudstone units (numbered) within the Boolgeeda Iron Formation (map and column after Martin, 1999). Sample 194504 (*) is from the broadly correlative section at Deepdale (Yeera Bluff). Age constraints refer to references cited in the text.

missing due to faulting (Williams et al., 1968). This sample (194504) is a mudstone and pyritic shale with outsized clasts.

2.2. Sample preparation for triple sulfur isotope analysis

Freshly broken hand samples were cut into chips with a diamond saw and prepared for doubly-polished petrographic thin sections. The thin sections were sub-divided with a diamond saw and re-cast together with sulfide standard grains in the same 2.54 cm epoxy rounds. A separate sulfide standards mount (GM4) was prepared using phases of equivalent compositions to the unknowns; these mounts were prepared following the methods described in Mojzsis et al. (2003). Reflected light microscopy images of these sample sections (Fig. S1) were acquired to note the location and size of pyrite grains for microanalysis. The sulfides were pre-characterized using back-scattered electron imaging and Wavelength Dispersive Spectroscopy (WDS) to identify the sulfide phase and characterize trace element (Ni, Co, and Zn) composition on the JEOL JXA-8600 electron microprobe at the University of Colorado at Boulder under operating conditions described in Papineau et al. (2005).

Pyrite grains >40 μm in diameter within the sample mounts were analyzed for triple sulfur isotopes (^{32}S, ^{33}S, ^{34}S) using the UCLA Cameca *ims*1270 ion-microprobe in multi-collector mode following previously described procedures (Mojzsis et al., 2003; Papineau et al., 2005). Briefly, a liquid nitrogen cold finger in the sample chamber was used to keep the partial pressure of water vapor low to decrease contribution from the isobar $^{32}SH^-$ in measurement of $^{33}S^-$. The mean analysis times were 360 s, of which 200 s was pre-sputtering, followed by 15 cycles of data acquisition at 10 s per cycle, and then 120 s of setup time between analyses so that total time per spot was ~8 min. Care was taken to ensure a uniform acquisition time at a particular primary beam current to maintain consistent pit depths for each analysis. The primary Cs^+ beam current was 3 nA defocused to a 20 μm spot. Measurements of samples

were punctuated by analysis of the GM4 standards mount (see above), and standard analyses were used to correct for instrument mass fractionation during each analysis session and to establish the terrestrial mass-fractionation line. The standard mount GM4 contains seven previously described and chemically characterized sulfides of varying compositions (pyrite, pyrrhotite, chalcopyrite, troilite; Papineau et al., 2005). Analyses were evaluated for drift in instrument conditions with time and divided into two sessions. The Δ^{33}S values are calculated according to the formula: $\Delta^{33}S_{CDT}$ (‰) = $1000 \cdot [(1 + \delta^{33}S / 1000) - (1 + \delta^{34}S / 1000)^{0.515}]$. Calculation of the slope of the MDF uncertainty band was based on the York least squares fitting method; this and other details of data reduction have been described elsewhere (Papineau et al., 2005).

2.3. Sulfide trace element analyses

Major and minor elements (Fe, S, Ni, As, and Cu) of the sulfides were acquired on thin sections using a JEOL 8900 electron microprobe at the University of Alberta (Edmonton, Canada). Instrumental parameters included a beam diameter of 3 μm, accelerating voltage of 15 kV, and beam current of 15 nA. Standards and corrections have been described elsewhere (Pecoits et al., 2009). The same instrument was used to collect secondary and backscattered electron images and elemental distribution maps (Fe, S, Au and Cu) of the sulfides reported herein. Quantitative in situ trace element analyses were made on the same sample mounts using a Quadrupole ICP-MS coupled to a laser ablation system at the University of Alberta. The NIST SRM 610 (~500 ppm Ni) was used as a standard for quantitative analysis. The NIST 610 and the sulfides were ablated using spot sizes of 160 and 60 μm, respectively, under previously described analytical conditions (Pecoits et al., 2009). The Glitter® (XP version, New Wave Research) laser ablation software was utilized for data reduction and concentration determinations. The results were normalized using the Mg and Fe contents acquired by

electron microprobe as internal standards. Regression analysis of trace element contents of pyrites utilized a reduced major axis equation appropriate for two independent variables to determine a slope, intercept and associated uncertainties for element–element co-variation (Rayner, 1985).

3. Results

Table 1 reports the δ^{33}S, δ^{34}S and Δ^{33}S[2] data for the in situ analysis of 30 individual pyrite grains from the sandstone and shale/mudstone units of the Boolgeeda Iron Formation. York least squares fitting regressions through ^{33}S/^{32}S against ^{34}S/^{32}S data obtained on standards and separated into two analytical sessions were used to determine the instrumental mass-dependent slope (λ) of 0.51352 for session 1 and 0.52681 for session 2 (Table S1). The measured (^{33}S/^{32}S)$_{CDT}$ ratios were 7.881×10^{-3} and 7.877×10^{-3} for sessions 1 and 2, respectively. The external errors are based on the reproducibility of the standards for δ^{33}S, δ^{34}S and Δ^{33}S, respectively at 2σ level were 0.76‰, 0.46‰ and 0.14‰ for analytical session 1 and 0.57‰, 0.40‰ and 0.20‰ for session 2. Average ^{32}S intensities on the faraday cup were 2.9×10^{8} cps (counts per second), but intensities smaller than 10^{8} cps were associated with large errors. Based on their low data quality, these analyses were excluded from our interpretations (Table 1).

Examples of common pyrite morphologies and different patterns in chemical compositions are shown in Fig. 2. Chemical and isotopic compositions of pyrites are discussed below grouped by hosting rock lithology (sandstone vs. shale/mudstone), and images of grain mounts showing the petrographic context of analyzed pyrite grains are provided in Fig. S1. The major mineralogy of analyzed sulfides is pyrite based on the elemental composition acquired by electron microprobe and laser ablation coupled to ICP-MS (LA-ICP-MS; Tables S2 and S3). Replicate analyses (n = 12) of the NIST 610 with a 60 μm LA-ICP-MS spot gave relative standard deviations of <10% (1σ level) and detection limits of 1.4 ppm for Co, 13.6 ppm for Ni, 14.9 ppm for Cu, 11.8 ppm for As and <200 ppm for Fe. Although zonation is generally lacking on backscattered electron images (Fig. S2), chemical heterogeneity within pyrite grains is evident based on variations in trace element concentrations acquired on 2 μm spots within pyrites by WDS (Table S3), and when these data are compared to 60 μm laser spots (Fig. 3F). Where more than one 20 μm spot per pyrite grain was analyzed for isotopic composition by ion microprobe, no S isotope heterogeneities were observed (Fig. S2).

3.1. Sandstone pyrites

Samples 190569, 190583 and 190578 are sandstones with a fine-grained matrix of quartz, sericite and chlorite collected from the Boundary Ridge location in the Duck Creek Syncline. Lonestones are up to 15–29 mm in diameter (Fig. S1). Samples 190569 and 190583 are from the lowermost sandstone unit, while sample 190578 is approximately 10 cm upsection (Fig. 1b). Pyrites in 190569 have several morphologies and textures (Fig. S2): subhedral (pyrites B, D and G), porous subhedral (pyrites C, E and F) and rounded with pores and inclusions (pyrite H). Sample 190583 contains rounded, inclusion-free pyrites (B, C, F and H), a rounded pyrite with inclusions (F) and a subhedral pyrite (E). The widest range in δ^{34}S values observed in this study is from sandstone samples: −9.1 to +3.5‰ (190569) and −6.6 to +5.9‰ (190583; Table 1). One Δ^{33}S value greater than +6‰ was observed in pyrite 190583B (Fig. 2F), but the other pyrites from this sample

Table 1
Multiple sulfur isotope data produced by ion microprobe for the Boolgeeda Iron Formation sulfides.

| Name	Phase	^{32}S avg. intensity (cps)	δ^{34}S$_{CDT}$ (‰)	$\pm 2\sigma$	δ^{33}S$_{CDT}$ (‰)	$\pm 2\sigma$	D^{33}S (‰)	$\pm 2\sigma$
Boundary Ridge								
190575A	py	1.72E+08	0.03	1.55	0.80	1.02	0.79	0.51
190575B	py	3.29E+08	−0.32	1.52	−0.16	0.95	0.01	0.35
190575C	py	3.45E+08	1.72	1.51	1.04	0.95	0.16	0.36
190575D[a]	py	5.64E+07	1.16	1.53	1.17	1.71	0.58	1.46
190575E	py	2.19E+08	0.98	1.52	0.09	1.02	−0.41	0.52
190575F	py	3.16E+08	1.05	1.51	0.63	0.95	0.10	0.36
190575G	py	2.90E+08	0.85	1.52	−0.01	1.44	−0.44	0.38
190575H[a]	py	3.97E+07	1.03	1.54	1.67	2.04	1.14	1.84
190575I	py	3.63E+08	1.36	1.52	0.75	0.96	0.06	0.37
190575J	py	1.56E+08	1.42	1.52	0.94	1.06	0.21	0.59
190578A@1	py	1.82E+08	−2.62	1.52	−1.20	1.05	0.16	0.57
190578A@2[a]	py	6.74E+07	−2.25	1.52	−0.69	1.52	0.48	1.23
190578C	py	2.82E+08	2.15	1.52	1.41	0.95	0.31	0.34
190578D	py	1.56E+08	1.30	1.52	0.91	1.03	0.25	0.54
190569B[a]	py	5.38E+07	3.27	1.18	−0.87	1.41	−2.64	1.23
190569C	py	2.34E+08	1.78	1.15	3.29	0.84	2.29	0.49
190569D	py	2.19E+08	2.18	1.15	0.80	0.85	−0.41	0.50
190569E@1	py	2.62E+08	2.69	1.15	3.28	0.89	1.81	0.56
190569E@2	py	2.86E+08	3.46	1.15	3.65	0.84	1.78	0.48
190569F@1	py	2.88E+08	−7.93	1.15	−4.16	0.82	−0.16	0.44
190569F@2	py	2.80E+08	−9.07	1.15	−4.77	0.83	−0.18	0.46
190569F@3	py	2.77E+08	−6.43	1.15	−3.31	0.87	−0.07	0.53
190569G	py	2.80E+08	−2.60	1.15	−1.38	0.84	−0.13	0.49
190569H	py	2.72E+08	−0.21	1.15	0.32	0.82	0.34	0.45
190583A	py	2.72E+08	1.14	1.52	0.35	0.95	−0.23	0.35
190583B@1	py	2.85E+08	5.88	1.52	9.29	0.94	6.27	0.33
190583B@2	py	3.10E+08	5.82	1.52	9.10	0.96	6.12	0.37
190583B@3	py	2.84E+08	5.61	1.52	9.10	0.96	6.22	0.37
190583C	py	2.82E+08	1.16	1.52	0.75	0.98	0.16	0.43
190583E	py	2.78E+08	−6.58	1.52	−3.30	0.97	0.11	0.39
Deepdale								
194504A@1	py	3.38E+08	−1.07	1.15	−0.48	0.84	−0.01	0.48
194504B@1	py	4.64E+08	1.23	1.15	0.92	0.82	0.20	0.45
194504C@1	py	4.74E+08	0.98	1.15	0.68	0.81	0.09	0.42
194504D@1[a]	py	5.12E+07	1.66	1.17	−1.79	1.44	−2.73	1.26
194504E@1	py	5.86E+08	0.55	1.15	0.59	0.81	0.22	0.43
194504E@2	py	5.85E+08	0.06	1.15	0.24	0.81	0.13	0.43
194504E@3	py	5.89E+08	0.11	1.15	0.37	0.81	0.23	0.43
194504E@4	py	5.52E+08	−3.95	1.15	−1.87	0.83	0.08	0.45
194504F@1	py	2.96E+08	0.97	1.15	0.42	0.81	−0.17	0.43
194504F@2	py	5.14E+08	0.11	1.15	0.31	0.81	0.18	0.43

[a] Analyses excluded from discussion due to low count rates.

recorded MDF-S (Table 1). Pyrites in sample 190569 record both MIF-S and MDF-S (−0.41 to +2.29‰; Table 1). Pyrites from these two samples contain variable amounts of trace elements (e.g. 14.4 to 7160 ppm As from sample 190583; Table S2). Molar Co and Ni concentrations are linearly correlated (log–log space) in sample 190583 (Table 2; Fig. 3A), but there is no correlation between either Ni and Co or Ni and As for sample 190569 (Fig. 3B; Table 2).

Sample 190578 contains euhedral pyrite (G, J, K) and subhedral, porous pyrite (A, C, E, H, L) in addition to a few rounded pyrites with inclusions (D and F; Fig. S2). The δ^{34}S values in sample 190578 range from −2.6 to +2.2‰, associated with Δ^{33}S values of +0.2 to +0.3‰ (Table 1). Pyrite 190578C has Cu hot spots visible in electron microprobe Cu maps (Fig. 2D). Linear correlations between molar Ni and Co in log–log space (Table 2; Fig. 3C) are significant, but those for Ni and As are not (Table 2).

3.2. Shale/mudstone pyrites

Sample 190575 was collected from a fissile shale with clasts at the Boundary Ridge location and is the uppermost stratigraphic sample analyzed in this study (Fig. 1). Pyrites analyzed for sulfur isotopes are euhedral to subhedral, and porous in form, 20–50 μm long and

---

[2] δ^{33}S and δ^{34}S values of a sample are calculated using the isotopic reference Canyon Diablo Troilite (CDT): δ^{3X}S$_{CDT}$ (‰) = [(^{3X}S / ^{32}S) / (^{3X}S / ^{32}S)$_{CDT}$ − 1] ∗ 1000, where X is 3 or 4. Δ^{33}S (‰) ≠ 0 represent deviation from mass-dependent fractionation of ^{33}S and ^{34}S: Δ^{33}S (‰) = 1000 ∗ [(1 + δ^{33}S / 1000) − (1 + δ^{34}S / 1000)$^\lambda$], and where λ is the experimentally determined mass-dependent slope.
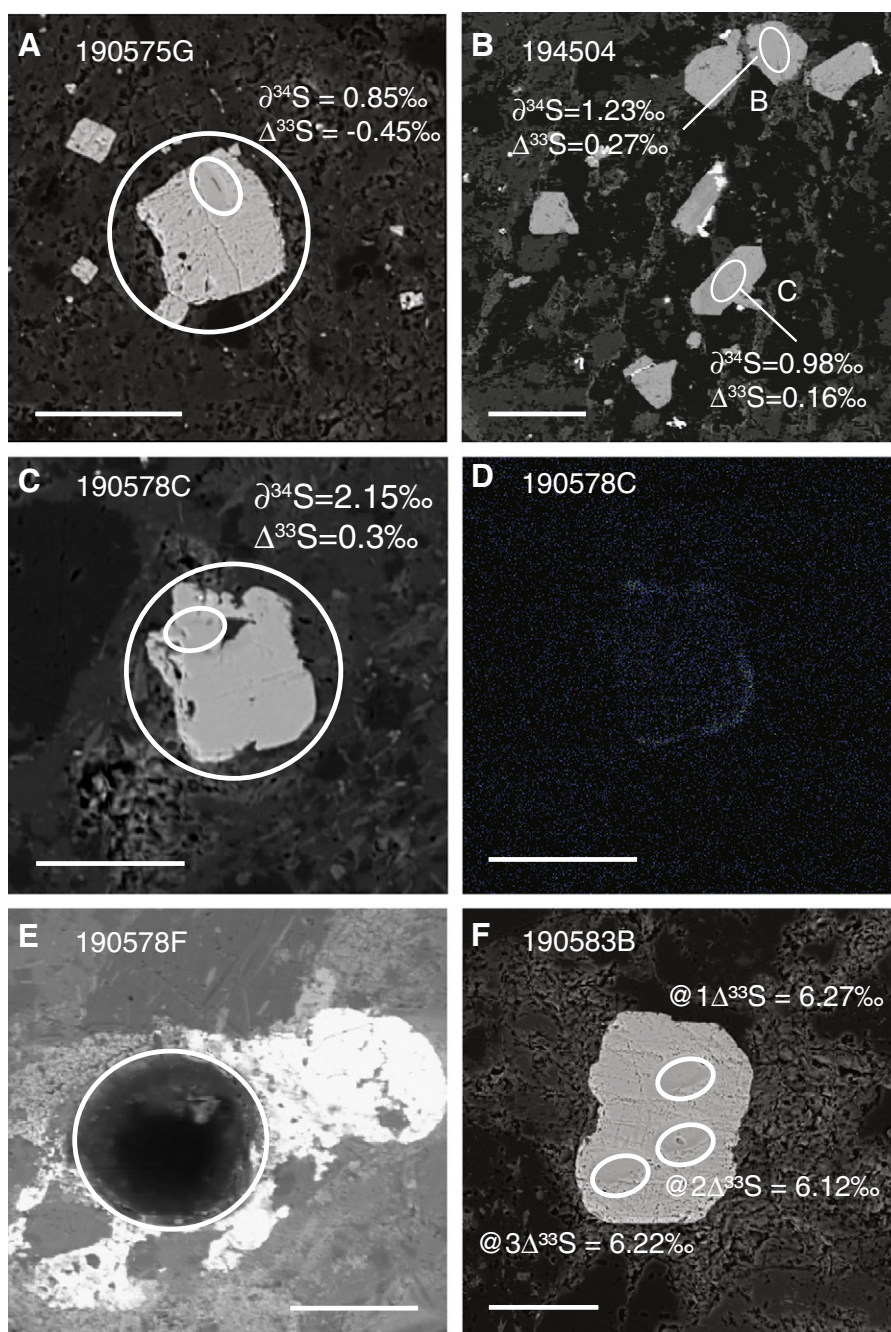
Fig. 2. Examples of pyrites discussed in the text, with representative textures, morphologies, chemical and isotopic compositions. A–B. Euhedral pyrites from shale/mudstone units. Bright regions on the rim of pyrite from sample 194504 in B. are possible base-metal sulfides. C. Rounded pyrite from sandstone sample 190578 and D. the same pyrite is enriched in Cu around the edge. E. Rounded pyrite from sample 190578 incorporating small clasts. F. Rounded pyrite from sample 190583 with the highest Δ^{33}S value found in this study. Small ovals denote ion microprobe pits; large circles indicate area targeted by laser ablation.

surrounded by smaller (<10 μm) euhedral pyrites (Fig. S2). Trace element concentrations in pyrite from sample 190575 showed little grain-to-grain variation (Ni < 300 ppm, Co < 130 ppm; Tables S2 and S3), except for grain 190575O (Fig. S2), which had anomalously high Ni (1166.66 ppm), Cu (562.44 ppm), As (2806.95 ppm) and Pb (1600.21 ppm) concentrations (Table S2). The linear correlation of molar Ni and Co on a log–log scale from sample 190575 pyrites (excluding 190575O) is significant (Table 2). The Δ^{33}S range in sample 190575 encompasses weak positive and negative values (-0.41 ± 0.52 to $+0.79 \pm 0.51$‰; Table 1), but the uncertainties lie within the MDF band (i.e. Δ^{33}S = 0 ± 0.3‰; Fig. 4A). However, positive MIF was observed for two grains of the same sample 190575 by Williford et al.

(2011) with an ion beam focused to a 10 μm diameter spot (Δ^{33}S: $+0.49 \pm 0.05$‰ and $+0.87 \pm 0.09$‰). Our range of δ^{34}S values for sample 190575 (-0.32 to $+1.72$‰; Table 1) using a 20 μm beam is also smaller than the previously published results using a 10 μm ion beam (-5.95 to $+2.35$‰; Fig. 5A).

Pyrite in the mudstone/pyritic shale sample (194504) from Deepdale is present in a matrix of fine-grained quartz, sericite and chlorite, and occurs as small euhedral and subhedral crystals from 20 to >100 μm in size and as disseminated pyrite aggregates (Figs. S1 and S2). The pyrites from sample 194504 analyzed by LA ICP-MS have Co contents from <1 to 133 ppm, whereas Co contents from pyrites within the sandstone samples are commonly up to several thousand ppm
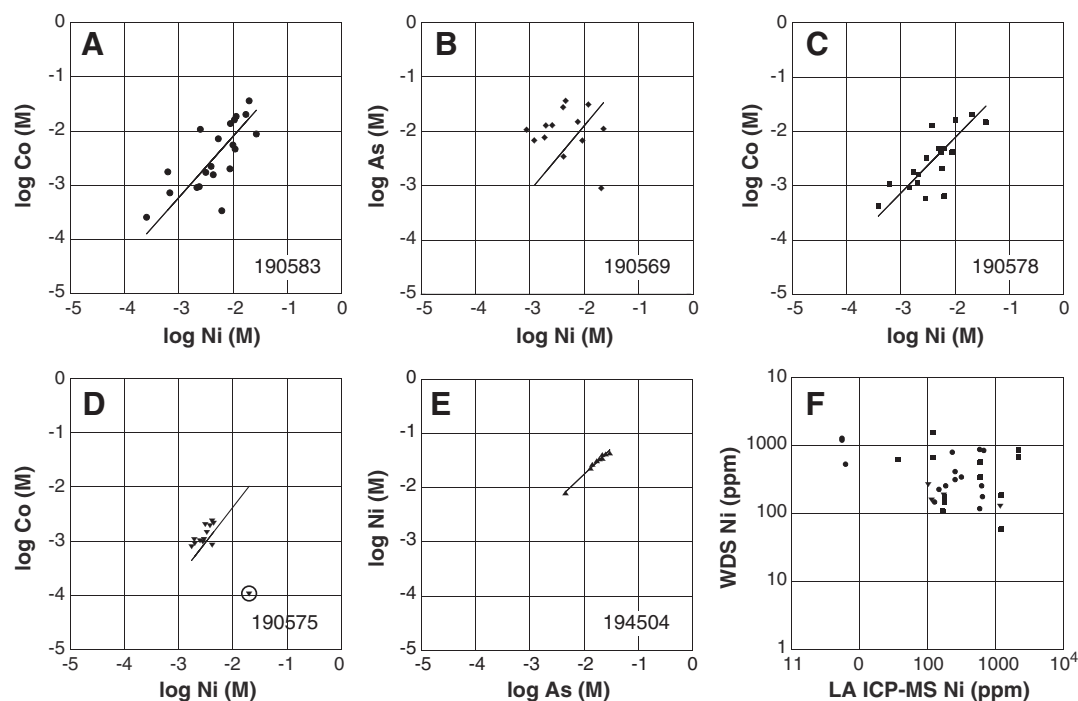
Fig. 3. Selected LA ICP-MS trace element data for pyrites from A–C. sandstone at Boundary Ridge, and shale/mudstone units at D. Boundary Ridge and E. Deepdale. Pyrite 190575O (circled) was excluded from the slope calculation. F. Variations in Ni concentration of individual pyrites acquired with 60 μm LA ICP-MS spots vs. 2 μm WDS spot analyses highlight the compositional heterogeneity of pyrites. Symbols correspond to A–E.

(Table S2 and S3). The Ni/As of 194504 pyrite is ~0.5 (Table S3), and molar Ni and As are linearly correlated in log–log space (Table 2; Fig. 3E). This co-variation between As and Ni was not evident when we evaluated the WDS analyses on pyrites from the same sample reported by Williford et al. (2011). The isotopic composition of the pyrite from sample 194504 ranges from -3.95 to $+1.23$‰ ($\delta^{34}S$; Table 1), which is similar to the range that we found in sample 190575, but incongruent with the data obtained with a 10 μm ion beam spot size for the same sample 194504 by Williford et al. (2011); their results show a remarkably large range (44‰) of $\delta^{34}S$ values (Fig. 4). Furthermore, no MIF-S was found in our pyrites from sample 194504; $\Delta^{33}S$ values range from -0.17 ± 0.43 to $+0.23 \pm 0.43$‰ (Table 1). The $\Delta^{33}S$ values (-0.83 ± 0.09 to $+0.68 \pm 0.06$‰) previously reported for the sample 194504 have a larger range and record MIF. The isotopic results for the two shale/mudstone samples analyzed in this study (Table 1) and with a smaller ion beam spot size by (Williford et al., 2011) plot

along the linear array of $\delta^{34}S$ vs. $\delta^{33}S$ values defined by the terrestrial fractionation line (TFL)[3] (Fig. 5A).

4. Discussion

To establish whether pyrite from the Boolgeeda Iron Formation diamictites at Boundary Ridge (Duck Creek Syncline) and Deepdale can resolve the uncertain but promulgated relationship of these units to the Meteorite Bore Member and hence to "global" Paleoproterozoic glaciations, it is necessary to establish whether pyrite is authigenic to the sediments. Detrital pyrites do not preserve information on the biogeochemical sulfur cycle during deposition of the sedimentary host rock. Petrographic study shows that the host lithologies in this study all contain detrital minerals (Fig. S1), and many of the analyzed pyrites are rounded (Fig. 2 and Fig. S2); a habit consistent with abrasion during surface transport. Fluvial transport of pyrite is possible in low-oxygen environments such as those that prevailed up to the time of the GOE, in cold environments with low chemical weathering rates, or under high erosion and sedimentation rates where it is rapidly buried (Rasmussen and Buick, 1999 and the references therein). While detrital pyrites generally show rounding, authigenic pyrites have a variety of morphologies, such as nodular, euhedral and framboidal. Euhedral pyrite, like some pyrite grains from the Boundary Range and Deepdale sections, grows slowly under diagenetic conditions from a few nucleation sites (i.e., growth-controlled) in contrast to framboids that apparently grow rapidly at a multitude of nucleation sites (i.e., nucleation controlled; Wang and Morse, 1996). However, euhedral habit is generally an inadequate criterion for assigning an authigenic origin to pyrite because it can also form in a variety of settings. The occurrence of euhedral crystals in lamina of sediments can signify an authigenic origin, but euhedral crystals forming along lithological contacts may also indicate formation from a late diagenetic or hydrothermal fluid (Guy et al., 2010). A more robust way to approach the problem is to take an

Table 2
Reduced Major Axis (RMA) slope, intercept and uncertainties for trace element co-variation in the Boolgeeda Iron Formation pyrites.

Sample		Co		As	
		RMA slope	RMA intercept	RMA slope	RMA intercept
Boundary Ridge					
190575[a]	Ni	**1.25 ± 0.27**	0.28 ± 0.11	(1.03 ± 0.24)	(0.52 ± 0.18)
		(1.29 ± 0.29)	(0.21 ± 0.22)		
190583	Ni	**1.13 ± 0.12**	0.16 ± 0.26	1.04 ± 0.2	0.13 ± 0.44
190569	Ni	1.20 ± 0.30	0.50 ± 0.41	**1.11 ± 0.25**	0.41 ± 0.34
190578	Ni	**1.02 ± 0.15**	−0.06 ± 0.23	1.44 ± 0.32	1.44 ± 0.48
Deepdale					
194504	Ni	2.84 ± 0.93	1.59 ± 0.64	**0.95 ± 0.05**	0.15 ± 0.03

Bold slopes are plotted in Fig. 3.
[a] Values in parenthesis include data from 190575O, the pyrite with high Ni, Cu and As concentrations.

---

[3] The terrestrial fractionation line is defined as $\delta^{33}S = 0.515 * \delta^{34}S$.

integrated approach that combines textural studies with trace element geochemistry. Trace elements, especially transition metals, generally reflect the composition of the host sediment (Raiswell and Plant, 1980; Guy et al., 2010) and ambient pore waters, so that enrichments could signify interaction with hydrothermal fluids that transported Co, Ni, and As at high temperature (Ohmoto and Goldhaber, 1997). In the following two sections, we combine the morphological, compositional and isotopic indicators from our analysis and those previously reported by Williford et al. (2011) for the same samples to unravel the genesis of pyrites from within the Boolgeeda Iron Formation at the Boundary Ridge and Deepdale sections.

4.1. Trace element and morphological indicators of pyrite genesis

Pyrites from the stratigraphically uppermost sample (190575) from the Boundary Ridge location of the Duck Creek Syncline, a fissile shale with pebble- to boulder-sized clasts, show a narrow range of Co, Ni and As concentrations relative to pyrites in the sandstone samples (Table S2; Fig. 3D), although pyrite 190575O has anomalously high Ni, Cu, As and Pb. The differences in elemental composition between shale and sandstone lithologies imply pyrite populations with different formational histories. The pyrites from sample 190575 all have a euhedral to subhedral habit (Fig. S2), and the narrow range of metal concentrations implies a growth from a fluid of uniform composition, suggesting that most pyrites within this sample formed in situ. Moreover, a subset of detrital cores appear to be overgrown during diagenesis; this is based on apparent zonation in some but not all pyrites from the same sample (Williford et al., 2011). Re–Os ages >2700 Ma for some pyrites from this sample are also evidence of a detrital contribution (Hickman and Van Kranendonk, 2012). The presence of pyrite with unique trace element contents (190575O) probably indicates the presence of some detrital pyrite within sample 190575.

Rounded grains and higher Co concentrations generally distinguish the pyrite in sandstones from those in the shale/mudstone units. Rounded pyrites with abrasion patterns are common in coarse-grained siliciclastic deposits (Guy et al., 2010). Ni and Co concentrations co-vary in pyrites from samples 190583 and 190578 (Fig. 3A and C), but not in pyrites from sample 190569 (Table 2). Co and Ni often co-vary in authigenic pyrites (Guy et al., 2010), because they both partition into the pyrite phase instead of forming Co- or Ni-sulfides during low-temperature pyrite formation (Morse and Arakaki, 1993). This supports the formation of detrital cores found within sandstone as authigenic minerals in a precursor sedimentary phase that was later eroded.

Conditions favoring authigenic pyrite formation were met in the Boundary Ridge section. Elemental heterogeneities are present in all pyrites from this location based on the variations in Ni concentrations observed with 60 μm LA ICP-MS spots vs. 2 μm electron microprobe spots (Fig. 3F). This is consistent with compositionally discrete cores observed in diamictite pyrites (Williford et al., 2011), and evidence of multiple generations of pyrite. Pyrite occasionally develops around clasts (i.e. 190578F; Fig. 2E), as a void-filling cement, which indicates pyrite formation at a shallow burial depth (Guy et al., 2010). The 2-isotope ion microprobe analyses reported on spots defocused to 2 μm in diameter (Fig. S6 of Williford et al., 2011) were used to map grains with visible zonation, and provide an independent validation that pyrite overgrowths formed within the host sediments from a sulfur source with a relatively homogenous $\delta^{34}S$ composition. Analyses acquired on rims or grains without rims show narrower ranges of $\delta^{34}S$ values than the entire sample set: 1–3.4‰ for shale 190575 (Fig. 4A) and 7.2–16.1‰ for sandstone 190578.

The co-variation between As and Ni concentrations in euhedral to subhedral pyrites from the mudstone/shale sample 194504 from the Deepdale location (Fig. 3E) is not present in pyrites from the other samples in this study (Table 2). Relatively constant As/Ni ratios with up to 2 wt.% As and 1 wt.% Ni have been documented in hydrothermal to metamorphic overgrowths of euhedral pyrite on detrital cores (England et al., 2002). Although we did not observe zonation in pyrites from sample 194504 (Fig. S2), both zonation and As, Ni and Co enrichment in rims were reported for some pyrites in the same sample 194504 by Williford et al. (2011). Furthermore, Re–Os ages >2450 Ma for pyrites from this sample point to a detrital origin (Hickman and Van Kranendonk, 2012). Some domains within individual pyrite grains of this sample display higher contrast in backscattered electron images, which implies enrichment in base metal sulfides (Fig. S2). One pyrite grain in particular (194504E) contained >12,000 ppm Pb (Table S2). Although no bright regions were observed in this pyrite, it is possible that some of the sample that was ablated for analysis contained galena (Fig. 2B). Pyrites in sample 194504 also have high Cu concentrations (up to 1825 ppm; Table S2), and although the pyrites from this sample were not scanned on electron microprobe for Cu, these enrichments could indicate that some amount of cuprite or cubanite is present. Distinct metal-sulfide phases precipitate from metal-enriched diagenetic pore waters prior to pyrite (Morse and Luther, 1999), and thus usually form the cores of sulfides (Guy et al., 2010). In this case, base metal-rich sulfides formed at the edges of, and in fractures of, pyrite grains B and C in sample 194504 (Fig. 2) are reminiscent of sulfides that form from hydrothermal fluids (Raymond, 1996). The pyrites from the
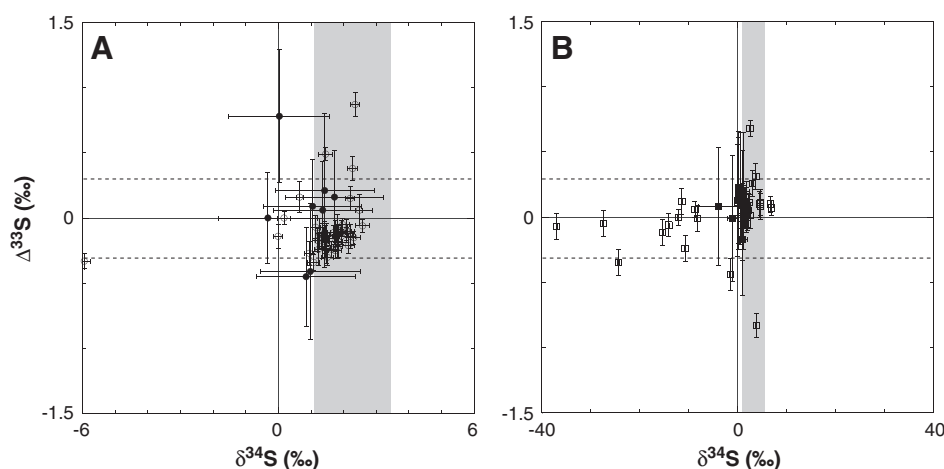
Fig. 4. A compilation of $\delta^{34}S$ vs. $\Delta^{33}S$ data from 20 μm spots (filled symbols; this study) and the 2 and 10 μm spots (open symbols; Williford et al., 2011) of pyrite from shale/mudstone samples analyzed by ion microprobe. a. Sample 190575 from Boundary Ridge has positive $\Delta^{33}S$ values for the range of $\delta^{34}S$ values acquired by 2 μm spot analyses (gray box) on euhedral and likely authigenic pyrite. b. Euhedral pyrites from the sample 194504 collected at Deepdale have both positive and negative $\Delta^{33}S$ values within the $\delta^{34}S$ range of authigenic rims acquired with 2 μm spot analyses (gray box). Dashed lines are borders for the MDF band.
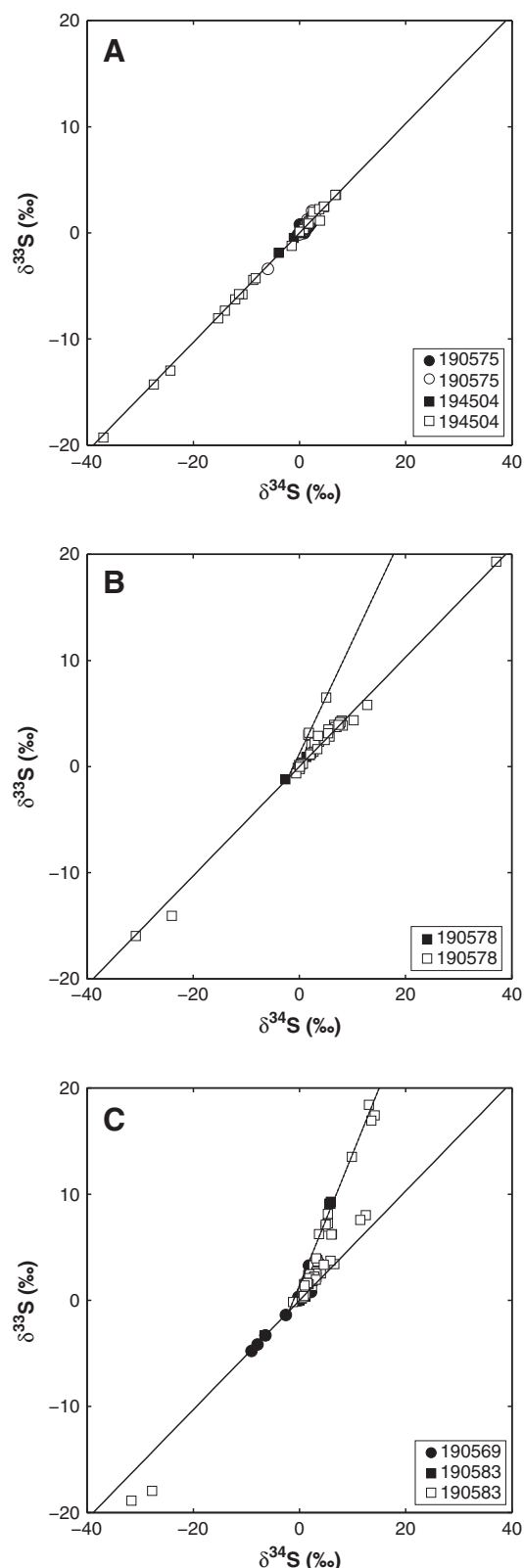
Fig. 5. Isotopic composition for 20 μm spots (filled symbols; this study) and 10 μm spots (open symbols; Williford et al., 2011) analyzed by ion microprobe. a. Shale/mudstone samples 190575 and 194504 plot along the TFL, but pyrites from 194504 have a larger range of δ³⁴S values. b. Pyrites from the sandstone sample 190578 plots along the TFL but also along δ³³S ≈ δ³⁴S + 1.3. c. Sandstone samples 190569 and 190583 contain pyrites with isotopic compositions that plot on the TFL as well as along δ³³S ≈ 1.2*δ³⁴S + 1.3.

shale facies (sample 190575) at the Boundary Ridge location display neither the As–Ni co-variation nor high Cu and Pb concentrations usually associated with hydrothermal pyrite, except for grain 190575O, of probable detrital origin. This could mean that metal-rich, late-stage hydrothermal alteration was localized to Deepdale. Deepdale is approximately 100 km along strike from the Boundary Ridge location (Hickman and Van Kranendonk, 2012) and in the direction of increased hydrothermal fluid flow associated with a ca. 2400 Ma thermo-tectonic event (Rasmussen et al., 2005). Rims around detrital cores have a small range of δ³⁴S values (0.6–5.4‰; Williford et al., 2011) either in the 10 μm dataset from that study or the 20 μm dataset presented here (Fig. 4B). This is consistent with rim growth from a relatively isotopically uniform metamorphic or hydrothermal fluid (England et al., 2002).

4.2. Sources of pyrite sulfur in the Boolgeeda Iron Formation

The presence of atmospherically-derived MIF sulfur, combined with two-sulfur isotopic compositions and trace element characteristics, suggests that some of the pyrite grains investigated here formed authigenically in a sedimentary environment. This conclusion has merit because Δ^{33}S signature does not change during sulfur incorporation into sulfide minerals (e.g. Ono et al., 2007), and this signature can be also maintained through metamorphism as sulfur self-diffusion in sulfides is very slow at low temperatures (Watson et al., 2009). The preservation of the primary sulfur isotopic signature is therefore expected for samples from the Boolgeeda Iron Formation, which did not reach a metamorphic grade higher than about prehnite-pumpellyite facies (Trendall, 1981).

Sulfur in pyrites from the Boundary Ridge and Deepdale sections within the Boolgeeda Iron Formation probably originated from several sources rather than solely from seawater. Pyrites with visible rims (as previously described by Williford et al., 2011) and chemical heterogeneities (this study) record several generations of sulfide growth. The pyrites from shales/mudstones with outsized clasts (samples 190575 and 194504) generally have weak positive and negative (194504) MIF-S values (Fig. 4A), which point to an input of atmospherically derived sulfur; both elemental sulfur aerosols (for example, S_8) with positive Δ^{33}S values and (seawater-soluble) sulfate aerosols with negative Δ^{33}S values (Ono et al., 2003).

Atmospherically-derived MIF-S signals can be diluted by dominantly MDF continentally-derived seawater sulfate or magmatic sulfur delivered from hydrothermal vents (Farquhar and Wing, 2003). Detrital pyrite cores in sample 194504 generally have negative δ³⁴S values, as do pyrites with no visible rims (Williford et al., 2011). Rims characterized in that study show a relatively small range of δ³⁴S values (+3.5 to +5‰; their Figs. S6 and S7), and they could have formed from a single fluid circulation event. Our range of δ³⁴S values for sample 190575 is also small (Fig. 5A), and except for one outlier value (−6‰; 10 μm ion microprobe spot by Williford et al., 2011), the combined data for the two different primary ion beam sizes – used to sample different size domains – fall within the δ³⁴S range of −0.32 to +3.4‰. Atmospherically-derived sulfur for authigenic pyrite formation is therefore inferred for sample 190575, the fissile shale with outsized clasts.

The sandstone samples record a larger range of Δ^{33}S values, including that for sample 190583, which is in excess of +6‰ (analysis reported herein) and greater than +11‰ (Williford et al., 2011). The data for this particular sample scatter along, as well as off, the terrestrial fractionation line (Fig. 4C). Our preferred interpretation is that this is consistent with multiple sources of sulfur. Combined with the rounded and abraded shape of these pyrites, their isotopic composition points to a detrital origin with different pyrite provenance (cf. Hofmann et al., 2009). The strongly positive Δ^{33}S values are a trademark signal for elemental sulfur aerosols as the sulfur source. This indicates that the detrital pyrites formed authigenically with atmospherically derived sulfur in their original source area, were later eroded, transported, and redeposited with diamictites in the Hamersley basin. Our sandstone-

hosted pyrite MIF S-isotope data along with the data from Williford et al. (2011) in Figs. 4B and C form a $\delta^{34}S$ vs. $\delta^{33}S$ array with a similar slope to that of authigenic Archean and pre-GOE Paleoproterozoic pyrites from the older Hamersley and Fortescue groups (Ono et al., 2003; Partridge et al., 2008). The Hamersley and Fortescue groups are therefore considered here as potential sources for the detrital pyrites and pyrite core domains in the Boolgeeda Iron Formation. Such arrays have been observed before for similarly-aged pyrites from South Africa and linked to a MIF sulfur source generated by SO_2 photolysis in the Archean anoxic atmosphere (Ono et al., 2009).

4.3. Implications for environmental conditions during deposition of the Boolgeeda Iron Formation

The persistence of MIF-S within detrital pyrites and pyrite grain cores in the Boolgeeda Iron Formation is firm evidence that the delivery of photochemical sulfur produced in an anoxic atmosphere to the Hamersley basin was operative, and therefore, that the precursor rocks were deposited at conditions where pO_2 was far below the calculated threshold of 10^{-5} present atmospheric level (PAL) that allows for preservation of the MIF-S signal (Pavlov and Kasting, 2002). That detrital pyrite exists within all units sampled furthermore validates this interpretation, because long-distance transport of pyrite implies (even if it does not prove) prevailing anoxic conditions (Rasmussen and Buick, 1999).

The pyrites from the uppermost fissile shale with outsized clasts analyzed in this study (190575) also contain sulfur with small but significant positive MIF-S (cf. Williford et al., 2011), and preserve the best evidence for authigenic pyrite from the Boundary Ridge section. The existence of detrital pyrite in this sample, based on Re–Os ages and the elemental heterogeneities cited above complicates the interpretation of whether atmospherically processed sulfur was supplied to the depositional site of the Boolgeeda Iron Formation. This is because $\Delta^{33}S$ data in our study were generally acquired in larger spots in the center of grains, which are most likely to sample detrital cores where they are present. To distinguish if MIF-S is authigenic, the $\delta^{34}S$ data are plotted against $\Delta^{33}S$ values for the 20 µm spot analyses in this study, and the 10 µm spot analyses of Williford et al. (2011) (Fig. 4A). In that study, additional two-isotope, 2 µm spot analyses were acquired on euhedral grains that lacked visible zonation, which defined a smaller range of $\delta^{34}S$ values (1.08–3.39‰) that may signify a more homogenous source of sulfur to authigenically formed pyrite within the host rocks. Positive MIF values (+0.87‰) are associated with this smaller range of $\delta^{34}S$ values (gray box in Fig. 5A), suggestive that atmospherically-derived sulfur was delivered to the depositional site of the shale. However, further triple isotope transects of these grains with a small beam (i.e. 10 µm) would be necessary to rule out the possibility that MIF-S was delivered within detrital cores.

A similar test for authigenic MIF-S was used with the data from the shale/mudstone sample 194504 from the Deepdale location (Fig. 4B). In this case, the two-isotope 2 µm data for visible rims in grains 15, 18, 24 and 45 (Fig. S6 of Williford et al., 2011) were used as a constraint for the $\delta^{34}S$ range (0.6–5.4‰; gray box in Fig. 4B) of authigenic pyrite. Both positive (0.68‰; grain 22) and negative (−0.83‰; grain 28) $\Delta^{33}S$ values characterize this range of $\delta^{34}S$ values, and occur in euhedral grains with no visible cores (Fig. S5 of Williford et al., 2011). This may signify a dominantly atmospheric sulfur source that was not diluted by sulfate produced by oxidative continental weathering during deposition of the Boolgeeda Iron Formation. If this interpretation is correct, the presence of positive and negative MIF in authigenic pyrite has important implications for the timing and tempo of oxidation. As discussed in the Introduction, pyrite formed prior to the transition to an oxic atmosphere is expected to bear both positive and negative $\Delta^{33}S$ values with a limited range of $\delta^{34}S$ values, whereas pyrite formed from an increasing seawater sulfate reservoir should retain only small positive $\Delta^{33}S$ values with larger negative $\delta^{34}S$ values.

Three $\delta^{34}S$ values lower than −20‰ associated with MDF-S were measured for sample 194504 via the 10 µm ion microprobe beam by Williford et al. (2011), and were used by the authors to infer an expanded sulfate reservoir during deposition. This assertion is at odds, however, with the presence of negative *and* positive MIF-S from likely authigenic pyrite of the same sample. An alternative explanation is that the small spot size reveals domains where the initial large fractionations resulting from microbial sulfate reduction (MSR) were produced even at low-sulfate concentrations. Micrometer-scale analyses of other geological samples have revealed small-scale variations in isotopic composition and large fractionations associated with sulfur metabolisms (e.g. 10‰ variation over 50 µm; Fike and Orphan, 2008) as well as demonstrably abiotic processes (England et al., 2002). The isotopic composition of the sulfide produced in experiments that were performed to characterize fractionation factors for MSR was determined on large product quantities via gas-source mass spectrometry (Habicht et al., 2002). This analytical approach homogenizes the compositional heterogeneities that may exist at the grain scale. High-resolution in situ analysis with a small size beam has not yet been performed on biologically-generated sulfide in biological experiments. Our 20 µm ion microprobe beam diameter yielded a much smaller range of $\delta^{34}S$ values for 190575 than that reported by Williford et al. (2011) and can be viewed as consistent with some degree of homogenization (Fig. 4A). It is noteworthy that in modern marine sediments, only a small fraction of pyrite that has ever been analyzed displays $\delta^{34}S$ values much below −30‰ (Ohmoto and Goldhaber, 1997). Furthermore, $\delta^{34}S$ values as low as −30‰ have not been observed in the Late Archean and earliest Paleoproterozoic Fortescue and Hamersley sulfides analyzed so far (Kakegawa et al., 1999, 2000; Ono et al., 2003; Kaufman et al., 2007; Partridge et al., 2008; Scott et al., 2011). Caution is therefore warranted when using $\delta^{34}S$ values from single small ion microprobe spot analyses to make inferences about the sulfate concentrations in the early Precambrian ocean. The composition of the bulk sample and of multiple pyrite grains must be interpreted alongside multiple sulfur isotope data during assessment of the seawater sulfate levels based on the magnitude of sulfur isotopic fractionation.

Data acquired using a 10 µm diameter ion beam (Williford et al., 2011) on sub-population of pyrites within the sandstone samples 190578 and 190583 shows highly negative $\delta^{34}S$ values (as low as −45.5‰); some of these values are associated with strikingly negative $\Delta^{33}S$ values (Fig. 5B, C). Highly negative $\delta^{34}S$ values in pyrites deposited to the Boolgeeda Iron Formation may reflect highly variable and increasing seawater sulfate level across the Archean–Paleoproterozoic boundary as suggested by Williford et al. (2011). Nonetheless, it is apparent that this interpretation conflicts with the highly negative $\Delta^{33}S$ values associated with the most negative $\delta^{34}S$ compositions obtained in that study. The sulfur with highly negative $\Delta^{33}S$ values must have been supplied from a low-oxygen atmosphere as sulfate aerosols rather than as sulfate derived from oxidative continental weathering, which is expected to impart minor *positive* $\Delta^{33}S$ values (Farquhar and Wing, 2003). A few studies report large ranges in $\delta^{34}S$ values for Archean pyrites (Grassineau et al., 2000; Shen et al., 2001; Hofmann et al., 2009) that in some cases also carried negative $\Delta^{33}S$ values (Hofmann et al., 2009; Shen et al., 2009). The $\delta^{34}S$ data reported for sample 190578 by Williford et al. (2011) spans almost 68‰. This is the largest range in $^{34}S/^{32}S$ ratios recorded for any sedimentary rock deposited prior to the expansion of the marine sulfate reservoir in the Neoproterozoic. One explanation for these data could be based on the nature of the sulfur metabolisms that were operative at that time. Large sulfur isotopic fractionations can occur in settings underlying oxic water where sulfur disproportionation occurs (Habicht and Canfield, 2001), or where sulfate reduction rates are exceedingly slow as in deep-sea sediments (Sim et al., 2011 and the references therein). A second option is that the atmospheric signal was preserved with minimal mixing with other sulfur pools within sediments, thereby explaining the negative $\Delta^{33}S$ and $\delta^{34}S$ values in pyrite.

4.4. Testing the correlation of the Boundary Ridge and Deepdale diamictites to the Meteorite Bore Member

The geological and environmental context under which siliciclastic sediments sampled at Boundary Ridge within the Duck Creek Syncline and Deepdale section were deposited is revealed by geochemical, petrographic, and trace element analyses of the various pyrites: oxygen was low enough to allow transport of detrital pyrite, sulfur was processed in an anoxic atmosphere as recorded by the presence of MIF-S, and oceanic sulfate was low enough to preserve the isotopic composition of atmospheric sulfur in pyrite. The data are consistent with deposition of the siliciclastic units at Boundary Ridge and Deepdale sections before the disappearance of MIF-S from the geological record in association with the GOE (Bekker et al., 2004; Papineau et al., 2007; Guo et al., 2009). However, these diamictites have previously been correlated to the Meteorite Bore Member of the Turee Creek Group (Martin, 1999) and were used to interpret the environmental conditions that prevailed during Paleoproterozoic glaciations and the GOE (Williford et al., 2011).

Several inconsistencies undermine the proposed correlation between the Meteorite Bore Member at the Hardey Syncline with diamictite-bearing units at the Boundary Ridge and Deepdale locations originally proposed by Martin (1999). No striated or faceted clasts that were originally reported for the Meteorite Bore Member (i.e. Trendall, 1975) have so far been observed at Boundary Ridge or at Deepdale, and clast-count data for massive diamictite at the Deepdale location and in the Meteorite Bore Member are dramatically different (Martin, 1999). Inference that Boundary Ridge and Deepdale diamictites represent glacial intervals rests on the presence of lonestones and the stratigraphic correlation to the Meteorite Bore Member of the Turee Creek Group in the Hardey Syncline. Alternatively, these diamictites could have been deposited as subaqueous debris-flows, similar to those that occur above the Boolgeeda Iron Formation at the Hardey Syncline (Krapez, 1996). Martin (1999) assigned diamictites at the Deepdale ("Yeera Bluff") location to the Boolgeeda Iron Formation. This was based on the fine laminations in the hosting banded iron formation that are similar to those which distinguish the Boolgeeda Iron Formation, and an upward gradation into siltstone. The Boolgeeda Iron Formation conformably underlies the Turee Creek Group in both the Duck Creek and Hardey Synclines, and the Meteorite Bore Member in the Hardey Syncline is sandwiched within shales of the Kungarra Formation more than 1000 m above the Boolgeeda Iron Formation (Krapez, 1996). Martin (1999) suggested that the highly asymmetric nature of the foreland basin is responsible for this stratigraphic discrepancy, but this implies that iron formation deposition was not synchronous throughout the basin. Iron formations are typically interpreted as condensed sections with minimal clastic and volcanic influxes, which are often correlative on the scale of greenstone belts (cf. Thurston et al., 2008).

It is difficult to explain why two sections less than 100 km apart and roughly along the depositional strike would have a correlative event unit positioned at dramatically different levels in the stratigraphy. Furthermore, units underlying and overlying the Boolgeeda Iron Formation are almost identical in the Hardey and Duck Creek Synclines, and carbonates in the basal part of the Turee Creek Group in the Duck Creek Syncline indicate shallow-water rather than a distal, deep-water depositional setting (Krapez, 1996). A more plausible explanation is that the stratigraphic levels with diamictites and lonestones in the Meteorite Bore Member and the Boolgeeda Iron Formation are in fact not correlative. While the former reflects a response to glaciation, the latter likely reflects the transition to the retro-arc basin, ending deposition in the extensional back-arc setting. Regardless of their exact correlation to each other, diamictites at the Boundary Ridge and Deepdale locations are older than the GOE based on the presence of detrital and authigenic pyrites with positive and negative MIF-S. Our data combined with those of Williford et al. (2011) suggests that only a few million years before the onset of the oldest Paleoproterozoic glaciation (corresponding to ~1 km thickness of the Turee Creek Group shales below the Meteorite Bore

Member), the atmosphere and, consequently, oceans were yet anoxic. The seawater sulfate reservoir was still small and atmospheric processing of the volcanically delivered SO_2 and H_2S gases continued to be the main source of sulfur to the oceans almost until the onset of the Paleoproterozoic Ice Ages.

5. Conclusions

To make full use of Archean sedimentary pyrite as a multifaceted paleo-environmental proxy, a suite of lithological, morphological, chemical and isotopic data must be combined to form a coherent picture of the depositional setting for any particular sample set. An in situ trace element and triple sulfur isotope dataset presented here reveals the origin of pyrite hosted in sandstone and shale/mudstone units within the Boolgeeda Iron Formation of the Hamersley Group. The pyrites from sandstone units of the Duck Creek Syncline are predominantly detrital with authigenic rim overgrowths (cf. Williford et al., 2011). Furthermore, the $\Delta^{33}S$ values of these detrital pyrite cores are consistent with their derivation from older sediments that recorded an earlier pool of atmospheric elemental sulfur that was formed in a photochemically active anoxic atmosphere with negligible contribution of continentally-derived seawater sulfate (i.e., prior to the GOE). The underlying units of the Fortescue and Hamersley groups are potential sources for this older pyrite. Unprecedented negative $\delta^{34}S$ values associated with a negative $\Delta^{33}S$ signal reported by earlier in situ ion microprobe analyses are consistent with the initial product of microbial sulfate reduction under limited concentrations of seawater sulfate supplied as photochemically fractionated sulfate aerosols from the atmosphere. This favors the notion that lower sulfate concentrations reigned in the earliest Paleoproterozoic until the GOE. A fissile shale with outsized clasts overlies the sandstone units and contains authigenic pyrite that preserves positive $\Delta^{33}S$ values, and positive and negative MIF-S occur at Deepdale, evidence that these units probably pre-date the GOE. These new sulfur isotope results further warrant a re-evaluation of the purported correlation between the studied units and what has been interpreted to be glaciogenic sediments of the Meteorite Bore Member within the Turee Creek Group. The Boolgeeda Iron Formation is stratigraphically below the Meteorite Bore Member, and diamictites lack strong indication of glacial origin. It remains unverified whether diamictites within the Boolgeeda Iron Formation represent Paleoproterozoic glaciation or tectonic change in the basin.

Supplementary data to this article can be found online at http://dx. doi.org/10.1016/j.chemgeo.2013.07.022.

References

Anbar, A.D., Duan, Y., Lyons, T.W., Arnold, G.L., Kendall, B., Creaser, R.A., Kaufman, A.J., Gordon, G.W., Scott, C., Garvin, J., Buick, R., 2007. A whiff of oxygen before the great oxidation event? Science 317, 1903–1906.

Barley, M.E., Pickard, A.L., Sylvester, P.J., 1997. Emplacement of a large igneous province as a possible cause of banded iron formation 2.45 billion years ago. Nature 385 (6611), 55–58.

Bekker, A., Kaufman, A.J., 2007. Oxidative forcing of global climate change: a biogeochemical record across the oldest Paleoproterozoic ice age in North America. Earth and Planetary Science Letters 258, 486–499.

Bekker, A., et al., 2001. Chemostratigraphy of the Paleoproterozoic Duitschland Formation, South Africa: implications for coupled climate change and carbon cycling. American Journal of Science 301 (3), 261–285.

Bekker, A., et al., 2004. Dating the rise of atmospheric oxygen. Nature 427 (6970), 117–120.

England, G.L., Rasmussen, B., Krapez, B., Groves, D.I., 2002. Palaeoenvironmental significance of rounded pyrite in siliciclastic sequences of the Late Archaean Witwatersrand Basin: oxygen-deficient atmosphere or hydrothermal alteration? Sedimentology 49 (6), 1133–1156.

Farquhar, J., Wing, B.A., 2003. Multiple sulfur isotopes and the evolution of the atmosphere. Earth and Planetary Science Letters 213 (1–2), 1–13.

Farquhar, J., Bao, H., Thiemens, M., 2000. Atmospheric influence of earth's earliest sulfur cycle. Science 289, 756–758.

Fike, D.A., Orphan, V.J., 2008. Micron-scale mapping of sulfur cycling across the oxycline of a cyanobacterial mat: a paired nanoSIMS and CARD-FISH approach. ISME Journal 2, 749–759.

Grassineau, N.V., et al., 2000. Antiquity of the biological sulphur cycle: evidence from sulphur and carbon isotopes in 2700 million-year-old rocks of the Belingwe Belt, Zimbabwe. Proceedings of the Royal Society of London Series A 268, 113–119.

Guo, Q., et al., 2009. Reconstructing Earth's surface oxidation across the Archean–Proterozoic transition. Geology 37 (5), 399–402.

Guy, B.M., Beukes, N.J., Gutzmer, J., 2010. Paleoenvironmental controls on the texture and chemical composition of pyrite from non-conglomeratic sedimentary rocks of the Mesoarchaean Witwatersrand Supergroup, South Africa. South African Journal of Geology 113 (2), 195–228.

Habicht, K.S., Canfield, D.E., 2001. Isotope fractionation by sulfate-reducing natural populations and the isotopic composition of sulfide in marine sediments. Geology 29 (6), 555–558.

Habicht, K.S., Gade, M., Thamdrup, B., Berg, P., Canfield, D.E., 2002. Calibration of sulfate levels in the Archean Ocean. Science 298 (5602), 2372–2374.

Halevy, I., Johnston, D.T., Schrag, D.P., 2010. Explaining the structure of the archean record of mass-independent sulfur isotope fractionation. Science 328, 204–207.

Hickman, A.H., Van Kranendonk, M.J., 2012. A Billion Years of Earth history: A Geological Transect through the Pilbara Craton and the Mount Bruce Supergroup—A Field Guide To Accompany 34th IGC Excursion WA-2. In: Australia, G.S.o.W. (Ed.), Geological Survey of Western Australia, East Perth, p. 66.

Hofmann, A., Bekker, A., Rouxel, O., Rumble, D., Master, S., 2009. Multiple sulphur and iron isotope composition of detrital pyrite in Archaean sedimentary rocks: a new tool for provenance analysis. Earth and Planetary Science Letters 286 (3–4), 436–445.

Johnston, D.T., 2011. Multiple sulfur isotopes and the evolution of Earth's surface sulfur cycle. Earth-Science Reviews 106, 161–183.

Kakegawa, T., Kawai, H., Ohmoto, H., 1999. Origins of pyrites in the 2.5 Ga Mt. McRae Shale, the Hamersley District, Western Australia. Geochimica et Cosmochimica Acta 62, 3205–3220.

Kakegawa, T., Kasahara, Y., Hayashi, K.-J., Ohmoto, H., 2000. Sulfur and carbon isotope analyses of the 2.7 Ga Jeerinah Formation, Fortescue Group, Australia. Geochemical Journal 34, 121–133.

Kaufman, A.J., et al., 2007. Late Archean biospheric oxygenation and atmospheric evolution. Science 317 (5846), 1900–1903.

Kirschvink, J.L., 1992. Late Proterozoic low-latitude global glaciation: the Snowball Earth. In: Schopf, J.W., Klein, C. (Eds.), The Proterozoic Biosphere. Cambridge University Press, Cambridge, pp. 51–52.

Kirschvink, J.L., et al., 2000. Paleoproterozoic snowball Earth: extreme climatic and geochemical global change and its biological consequences. Proceedings of the National Academy of Sciences 97 (4), 1400–1405.

Konhauser, K.O., Lalonde, S.V., Planavsky, N., Pecoits, E., Lyons, T.W., Mojzsis, S.J., Rouxel, O.J., Barley, M.E., Rosiere, C., Fralick, P.W., Kump, L.R., Bekker, A., 2011. Aerobic bacterial pyrite oxidation and acid rock drainage during the Great Oxidation Event. Nature 478, 369–373.

Kopp, R.E., Kirschvink, J.L., Hilburn, I.A., Nash, C.Z., 2005. The Paleoproterozoic snowball Earth: a climate disaster triggered by the evolution of oxygenic photosynthesis. Proceedings of the National Academy of Sciences of the United States of America 102 (32), 11131–11136.

Krapez, B., 1996. Sequence stratigraphic concepts applied to the identification of basin-filling rhythms in Precambrian successions. Australian Journal of Earth Sciences 43, 355–380.

Krapež, B., Barley, M.E., Pickard, A.L., 2003. Hydrothermal and resedimented origins of the precursor sediments to banded iron formation: sedimentological evidence from the Early Palaeoproterozoic Brockman Supersequence of Western Australia. Sedimentology 50 (5), 979–1011.

Martin, D.M., 1999. Depositional setting and implications of Paleoproterozoic glaciomarine sedimentation in the Hamersley Province, Western Australia. Geological Society of America Bulletin 111 (2), 189–203.

Mojzsis, S.J., 2007. Sulphur on the Early Earth. In: Van Kranendonk, M.J., Smithies, R.H., Bennett, V.C. (Eds.), Earth's Oldest Rocks. Elsevier, Amsterdam, pp. 923–970.

Mojzsis, S.J., Coath, C.D., Greenwood, J.P., McKeegan, K.D., Harrison, T.M., 2003. Mass-independent isotope effects in Archean (2.5 to 3.8 Ga) sedimentary sulfides determined by ion microprobe analysis. Geochimica et Cosmochimica Acta 67 (9), 1635–1658.

Morse, J.W., Arakaki, T., 1993. Adsorption and coprecipitation of divalent metals with mackinawite (FeS). Geochimica et Cosmochimica Acta 57 (15), 3635–3640.

Morse, J.W., Luther III, G.W., 1999. Chemical influences on trace metal–sulfide interactions in anoxic sediments. Geochimica et Cosmochimica Acta 63 (19–20), 3373–3378.

Müller, S.G., Krapež, B., Barley, M.E., Fletcher, I.R., 2005. Giant iron-ore deposits of the Hamersley province related to the breakup of Paleoproterozoic Australia: new insights from in situ SHRIMP dating of baddeleyite from mafic intrusions. Geology 33 (7), 577–580.

Ohmoto, H., Goldhaber, M., 1997. Sulfur and carbon isotopes. In: Barnes, H.D. (Ed.), Geochemistry of Hydrothermal Ore Deposits. John Wiley and Sons, New York, pp. 517–611.

Ono, S., et al., 2003. New insights into Archean sulfur cycle from mass-independent sulfur isotope records from the Hamersley Basin, Australia. Earth and Planetary Science Letters 213 (1–2), 15–30.

Ono, S., Shank III, W.C., Rouxel, O.J., Rumble III, D., 2007. S-33 constraints on the seawater sulfate contribution in modern seafloor hydrothermal vent sulfides. Geochimica et Cosmochimica Acta 71, 1170–1182.

Ono, S., Beukes, N.J., Rumble, D., 2009. Origin of two distinct multiple-sulfur isotope compositions of pyrite in the 2.5 Ga Klein Naute Formation, Griqualand West Basin, South Africa. Precambrian Research 169 (1), 48–57.

Papineau, D., Mojzsis, S.J., Coath, C.D., Karhu, J.A., McKeegan, K.D., 2005. Multiple sulfur isotopes of sulfides from sediments in the aftermath of Paleoproterozoic glaciations. Geochimica et Cosmochimica Acta 69 (21), 5033–5060.

Papineau, D., Mojzsis, S.J., Schmitt, A.K., 2007. Multiple sulfur isotopes from Paleoproterozoic Huronian interglacial sediments and the rise of atmospheric oxygen. Earth and Planetary Science Letters 255, 188–212.

Partridge, M.A., Golding, S.D., Baublys, K.A., Young, E., 2008. Pyrite paragenesis and multiple sulfur isotope distribution in late Archean and early Paleoproterozoic Hamersley Basin sediments. Earth and Planetary Science Letters 272 (1–2), 41–49.

Pavlov, A.A., Kasting, J.F., 2002. Mass-independent fractionation of sulfur isotopes in Archean sediments: strong evidence for an anoxic Archean atmosphere. Astrobiology 2 (1), 27–41.

Pecoits, E., et al., 2009. Petrography and geochemistry of the Dales Gorge banded iron formation: paragenetic sequence, source and implications for paleo-ocean chemistry. Precambrian Research 172 (1–2), 163–187.

Philippot, P., et al., 2007. Early Archaean microorganisms preferred elemental sulfur, not sulfate. Science 317 (5844), 1534–1537.

Philippot, P., van Zuilen, M., Rollion-Bard, C., 2012. Variations in atmospheric sulphur chemistry on early Earth linked to volcanic activity. Nature Geoscience 5, 668–674.

Raiswell, R., Plant, J., 1980. The incorporation of trace elements into pyrite during diagenesis of black shales, Yorkshire, England. Economic Geology 75, 684–699.

Rasmussen, B., Buick, R., 1999. Redox state of the Archean atmosphere: evidence from detrital heavy minerals in ca. 3250–2750 Ma sandstones from the Pilbara Craton, Australia. Geology 27 (2), 115–118.

Rasmussen, B., Fletcher, I.R., Sheppard, S., 2005. Isotopic dating of the migration of a low-grade metamorphic front during orogenesis. Geology 33 (10), 773–776.

Raymond, O.L., 1996. Pyrite composition and ore genesis in the Prince Lyell copper deposit, Mt Lyell mineral field, western Tasmania, Australia. Ore Geology Reviews 10 (3,Äì6), 231–250.

Rayner, J.M.V., 1985. Linear relations in biomechanics: the statistics of scaling functions. Journal of Zoology (London) (A) 206, 415–439.

Reinhard, C.T., et al., 2013. Proterozoic ocean redox and biogeochemical stasis. Proceedings of the National Academy of Sciences of the United States of America 110 (14), 5357–5362.

Scott, C.T., et al., 2011. Late Archean euxinic conditions before the rise of atmospheric oxygen. Geology 39 (2), 119–122.

Shen, Y., Buick, R., Canfield, D.E., 2001. Isotopic evidence for microbial sulphate reduction in the early Archaean era. Nature 410, 77–81.

Shen, Y., Farquhar, J., Masterson, A., Kaufman, A.J., Buick, R., 2009. Evaluating the role of microbial sulfate reduction int he early Archean using quadruple sulfur isotopes systematics. Earth and PLanetary Science Letters 279, 383–391.

Sim, M.S., Bosak, T., Ono, S., 2011. Large sulfur isotope fractionation does not require disproportionation. Science 333, 74–77.

Takehara, M., Komure, M., Kiyokawa, S., Horie, K., Yokoyama, K., 2010. Ditrital zircon SHRIMP U–Pb age of the 2.3 Ga diamictites of the Meteorite Bore Member in the South Pilbara, Western Australia. In: Taylor, I.M., Knox-Robinson, C.M. (Eds.), Fifth International Archean Symposium. Fifth International Archean Symposium Abstracts: Geological Survey of Western Australia, Record 2012/18, Perth, Western Australia, pp. 223–224.

Thurston, P.C., Ayer, J.A., Goutier, J., Hamilton, M.A., 2008. Depositional gaps in Abitibi greenstone belt stratigraphy: a key to exploration for syngenetic mineralization. Economic Geology 103 (6), 1097–1134.

Trendall, A.F., 1975. Striated and Faceted Boulders from the Turee Creek Formation—Evidence for a Possible Huronian Glaciation on the Australian Continent.

Trendall, A.F., 1981. The lower Proterozoic Meteorite Bore Member, Hamersley Basin, Western Australia. In: Hambrey, M.J., Harland, W.B. (Eds.), Earth's Pre-Pleistocene Glacial Record. Cambridge University Press, Cambridge, pp. 555–557.

Ueno, Y., Ono, S., Rumble, D., Maruyama, S., 2008. Quadruple sulfur isotope analysis of ca. 3.5 Ga Dresser Formation: new evidence for microbial sulfate reduction in the early Archean. Geochimica et Cosmochimica Acta 72 (23), 5675–5691.

Wang, Q., Morse, J.W., 1996. Pyrite formation under conditions approximating those in anoxic sediments I. Pathway and morphology. Marine Chemistry 52 (2), 99–121.

Watson, E.B., Cherniak, D.J., Frank, E.A., 2009. Retention of biosignatures and mass-independent fractionations in pyrite: self-diffusion of sulfur. Geochimica et Cosmochimica Acta 73 (16), 4792–4802.

Williams, I.R., Ryan, G.R., Halligan, R., 1968. Yarraloola, WA Sheet SF50-6. Bureau of Mineral Resources, Geology and Geophysics, Department of National Development, Canberra.

Williford, K.H., Van Kranendonk, M.J., Ushikubo, T., Kozdon, R., Valley, J.W., 2011. Constraining atmospheric oxygen and seawater sulfate concentrations during Paleoproterozoic glaciation: in situ sulfur three-isotope microanalysis of pyrite from the Turee Creek Group, Western Australia. Geochimica et Cosmochimica Acta. http://dx.doi.org/10.1016/j.gca.2011.07.010.

Wing, B.A., Brabson, E., Farquhar, J., Kaufman, A.J., Rumble III, D., 2002. $\Delta^{33}S$, $\delta^{34}S$ and $\delta^{13}C$ constraints on the Paleoproterozoic atmosphere during the earliest Huronian glaciation. Geochimica et Cosmochimica Acta 66, A840.

Wing, B.A., et al., 2004. Atmospheric Chemistry of SO_2 during the Earliest Huronian Glaciation. GSA Abstracts with Programs, p. 339.